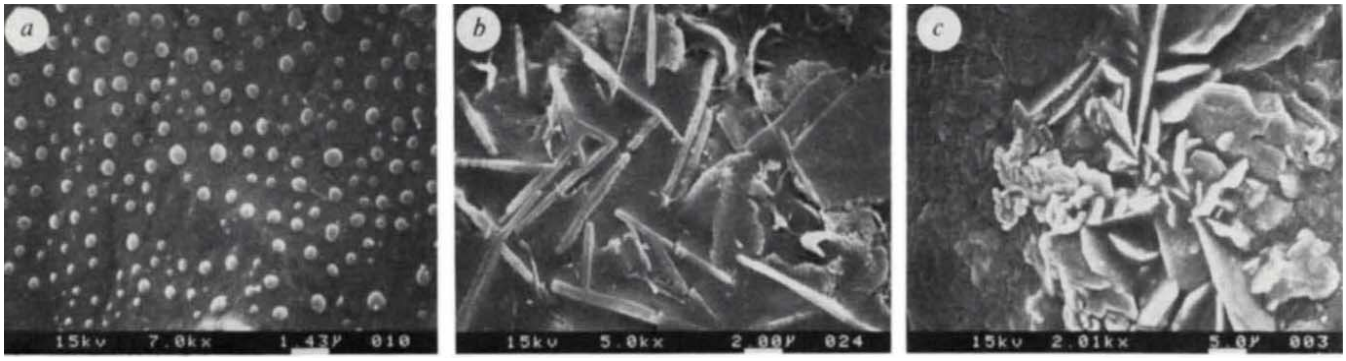

FIG. 3 *a*, Scanning electron micrograph of a polyethyleneoxide film after *in situ* synthesis of CdS at 120 °C and 6 h annealing at 200 °C. *b*, Scanning electron micrograph of a polyethylene oxide film after *in situ* synthesis of CdS using the same conditions as *a*, but the presence of 0.06 M 2,2′,2″-triaminotriethylamine. *c*, Scanning electron micrograph of a polyethylsuccinate film after *in situ* synthesis of CdS at 56 °C.

solution 0.03 M in the surfactant sodium di(2-ethylhexyl)-sulphosuccinate (AOT) an even more ordered environment can be induced in the semicrystalline polymer matrix. The room-temperature CdS product is considerably altered. A few crystals of bipyramidal habit, of the order of 1 μm on an edge, are formed. The number of these crystals depends strongly on the AOT concentration, and reducing the concentration greatly reduces their number. In all cases, however, many cubic single crystals, ~200 nm on an edge, were also formed throughout the film (Fig. 2*b*). The crystals were orientated such that all displayed the allowed *hk*0 reflections in their electron diffraction patterns, but we saw no traces of the allowed reflections with $l \neq 0$. The crystals were thus uniformly aligned with a crystallographic fourfold axis (the [001] zone) perpendicular to the plane of the organic film (Fig. 2*c*). Also, single-crystal electron-diffraction patterns of many individual crystals, as well as powder electron-diffraction patterns of different areas of the films containing many crystals, indicate that the crystals had the rock-salt structure (Fig. 2*c*), a phase previously seen in CdS only at high pressures[16]. A recent study of CdS particles synthesized *in vivo* by yeast cells also indicated that the biomineralized particles may adopt this structure[17,18]. In our case, the AOT could assemble on the film's surface with its polar sulphonate head group interacting with the polar PEO, and the non-polar alkyl tail extending into the octane solution. Selective crystallization and orientation could then be mediated by the head group's interactions with polymer-bound Cd^{2+} ions, as was seen in crystallizations from solutions with a Langmuir–Blodgett layer of surfactant on the air/liquid interface[19,20].

Besides matrix mediation of nucleation, two other key features of biomineralization are control of ion flux at the matrix interface, and growth and habit modification by soluble molecules within the matrix[15]. We see analogous effects in this synthetic system. Particle or crystal size of the CdS in the PEO film can be varied by altering the initial $CdCl_2$ concentration: we have obtained particle sizes from 2 nm to 2 μm. Crystal habit is similarly altered by addition of ligands. For example, the spherical morphology found in 8% CdS/PEO synthesized at 120 °C and annealed at 200 °C for 6 h (Fig. 3*a*) changes to a fibrous one when the reaction occurs in the presence of 0.06 M 2,2′,2″-triaminotriethylamine (Fig. 3*b*). These fibres closely resemble the ordered chains of magnetite biosynthesized in magnetotactic bacteria, as they are also composed of small crystallites linearly arranged[21]. Use of a different crystalline polymer matrix also alters the CdS product morphology (Fig. 3*c*).

The control of the inorganic phase's size, morphology, crystalline phase and crystallographic orientation that this biomimetic synthesis allows would be highly desirable in fabricating composite materials with technological applications[1,7,22]. We are now applying this synthetic method to the fabrication of other inorganic materials in ordered arrays within polymer matrices. □

Received 11 September; accepted 20 November 1990.

1. Mann, S. *Nature* **322,** 119–124 (1988).
2. Mann, S., Heywood, B. R., Rajam, S. & Birchall, J. D. *Nature* **334,** 692–694 (1988).
3. Azoz, N., Calvert, P. D., Kadim, M., McCaffery, A. J. & Seddon, K. *Nature* **344,** 49–51 (1990).
4. Berman, A., Addadi, L. & Weiner, S. *Nature* **331,** 546–548 (1988).
5. Fendler, J. H. *Chem. Rev.* **87,** 877–899 (1987).
6. Andres, R. P. *et al. J. Mater. Res.* **4,** 704–736 (1989).
7. Calvert, P. & Mann, S. *J. Mater. Sci.* **23,** 3801–3815 (1988).
8. Herron, N. *et al. J. Am. chem. Soc.* **111,** 530–540 (1989).
9. Abel, E. W. & Jenkins, C. R. *J. Organometall. Chem.* **14,** 285–287 (1968).
10. Rossetti, R., Ellison, J., Gibson, J. M. & Brus, L. E. *J. chem. Phys.* **80,** 4464–4469 (1984).
11. Yuan, T., Cabasso, I. & Fendler, J. H. *Chem. Mater.* **2,** 226–229 (1990).
12. Xu, S., Zhao, X. K. & Fendler, J. H. *Adv. Mater.* **2,** 183–185 (1990).
13. Steigerwald, M. L. *et al. J. Am. chem. Soc.* **110,** 3046–3050 (1988).
14. Iwamoto, I., Saito, Y., Isihara, H. & Tadokoro, H. *J. Polym. Sci.* **6,** 1509–1525 (1968).
15. Mann, S. *Struct. Bond. (Berlin)* **54,** 125–174 (1983).
16. Osugi, J., Shimuzu, K., Nakamura, T. & Onoder, A. *Rev. Phys. Chem. Jap.* **36,** 59–73 (1966).
17. Dameron, C. T. *et al. Nature* **338,** 596–597 (1989).
18. Dameron, C. T. & Winge, D. R. *Inorg. Chem.* **29,** 1343–1348 (1990).
19. Landau, E. H., Levanon, M., Leiserowitz, L., Lahav, M. & Sagiv, J. *Nature* **318,** 353–356 (1985).
20. Mann, S. J., Heywood, B. R., Rajam, S. & Birchall, J. D. *Nature* **334,** 692–695 (1988).
21. Mann, S., Frankel, R. B. & Blakemore, R. P. *Nature* **310,** 405–407 (1985).
22. Mann, S. *et al. Adv. Mater.* **2,** 257–261 (1990).

ACKNOWLEDGEMENTS. We thank I. Williams, C. Randall and G. Farber for advice on crystallography. This work was supported by the Petroleum Research Fund.

Shock-induced martensitic phase transformation of oriented graphite to diamond

D. J. Erskine & W. J. Nellis

Lawrence Livermore National Laboratory, University of California, Livermore, California 94550, USA

ONE important method of diamond synthesis is shock compression of graphite and other forms of carbon to high pressures and temperatures, and subsequent quenching to yield metastable diamond. This process, which occurs in microseconds, happens naturally in the impact of meteors[1,2], within products of explosives[3,4], and by explosive compression of powders[5,6]. A major unresolved issue is whether the shock-induced phase transition of graphite to diamond is martensitic or diffusive. The relation between the crystal structures of graphite and hexagonal diamond suggests that the phase transition should be fast and martensitic if shock pressure is applied parallel to the *c* axis (normal to the basal planes) of the graphite crystal structure. Here we report measurements of shock-wave histories for this transition which

show that it occurs in ~10 ns. These results imply that the transformation from graphite to diamond is martensitic for temperatures substantially lower than the melting temperature. We observe an unexpectedly large sensitivity of kinetics to sample morphology. As well as answering questions concerning the physical nature of the transformation, our results are relevant to optimization of diamond yield in industrial synthetic methods.

Shock[6-8] and static[9] high-pressure synthesis of diamond from graphite produces hexagonal (lonsdaleite) and cubic diamond. Higher temperatures increase the yield of the cubic phase[7-9]. Comparison of the relative crystallographic orientations of product and reactant phases of shock-synthesized diamond particles provides evidence for a martensitic transformation from hexagonal graphite to hexagonal diamond[7] for temperatures <2,000 K, which are low compared with the melting temperature of carbon (~4,000 K at ~20 GPa)[9]. For temperatures of 3,000–4,000 K, only cubic diamond is observed, regardless of the initial carbon phase, indicating that the transition is reconstructive and diffusive at these temperatures. At intermediate temperatures, in which a mixture of the two phases is produced, there is some microstructural evidence that shock synthesis of cubic diamond from graphite has two steps: a martensitic transformation to lonsdaleite, followed by a second transformation, possibly martensitic, from the hexagonal to the cubic phase[7]. Thus these microstructural results indicate that the phases produced are determined by the transformation mechanism, which in turn is strongly dependent on temperature.

A major unresolved issue is why, if the transition from graphite to hexagonal diamond is martensitic, the transformation has not been observed in real-time shock experiments with nanosecond time resolution. As systematic atomic displacements take hexagonal graphite into hexagonal diamond, this transformation is expected to be martensitic and therefore should happen on application of shock pressure over a timescale of a few nanoseconds. Observation of a fast transformation would provide definitive confirmation of a martensitic mechanism. Time-resolved observations may also provide clues for technological improvements such as optimizing the efficiency of transforming graphite and retaining diamond.

Although real-time shock-compression experiments have been performed previously, interpretation of these data is not unambiguous, largely because of the initial microstructures of the graphite specimens: the experiments were performed with pyrolytic and porous graphite. Pyrolytic graphite is a quasi-single-crystal form with the basal plane of the hexagonal crystal structure oriented preferentially in the plane of the constituent platelet grains, such that the specimens have a mosaic structure with the c axis of each crystallite distributed a few degrees about the specimen normal. Misalignment of crystallites in the mosaic structure may exert a heterogeneous influence on the transformation mechanism. Porous graphite is a compact of powder particles with porosity up to a few tens per cent. When porous material is shock-compressed, material immediately around collapsed pores is shock-heated to much higher temperatures than the material further from the pores[10], with the result that phase-transformation studies of porous graphite are complicated by spatially heterogeneous temperature distributions and thus again by possible spatial distributions of the transformation mechanism.

A martensitic transformation should yield a well defined onset pressure P_{0t} of the transition. Previous shock-wave equation-of-state data[11-15] for pyrolytic and porous graphite, however, show a range of P_{0t}, with porous samples exhibiting a lower P_{0t} (~20 GPa) than dense pyrolytic ones. This variation in P_{0t} has been attributed[16] to a thermally activated diffusive (rather than martensitic) transformation driven by higher shock temperatures in porous specimens.

The most direct method of observing shock-induced phase transitions is to measure time histories of shock waves. Because the graphite-to-diamond transition involves a relatively large volume change, the shock-wave history should show two steps (a 'two-wave' structure) in shock pressure or material velocity[17]. The first step corresponds to shock compression of graphite to P_{0t}, and the second corresponds to a rise in pressure to the phase-transformed state. Shear stress, which exists in shocked solids, is expected to drive this transition quickly by inducing displacive shear motion between lattice planes so as to produce the hexagonal-diamond stacking sequence. Thus for martensitic transitions, the second rise should be rapid, lasting perhaps several nanoseconds. A two-wave structure has been observed in porous graphite[18], but because of the heterogeneous nature of shock heating in such specimens, these results are not definitive in determining the transformation mechanism.

We shock-compressed highly oriented pyrolytic graphite parallel to the c axis and measured the shock-wave velocity profile. Shock waves were generated by impact of a copper disk accelerated by a two-stage light-gas gun to velocities of 2.6–3.4 km s^{-1}. The copper disk struck an aluminium baseplate on which a graphite specimen was mounted. The specimen was backed by a LiF window through which a laser beam was reflected off the rear surface of the graphite. As LiF has a shock impedance close to that of graphite, the perturbation of the shock wave by the interface is relatively small. The laser is the probe beam of our VISAR interferometer[19], which measures the velocity of the graphite–LiF interface to 0.1% with a time resolution of 2–3 ns.

Two grades of pyrolytic graphite (ZYB and ZYH) obtained from Union Carbide were used. The specimens were 2.5 mm thick and at least 13 mm square. The grades are distinguished by the value of β, the angular width of the (002) X-ray diffraction peak, which measures the spread of misalignment of the crystallite c axes. For the high- and low-grade samples β is 0.8° and 3.5° respectively. The high-grade samples had a shiny metallic lustre, and the low-grade ones had a dull 'pencil-lead' appearance. The densities were 2.254 and 2.262 g cm^{-3} for the high and low grades, respectively, which are very near the handbook value[20] of 2.265 g cm^{-3}.

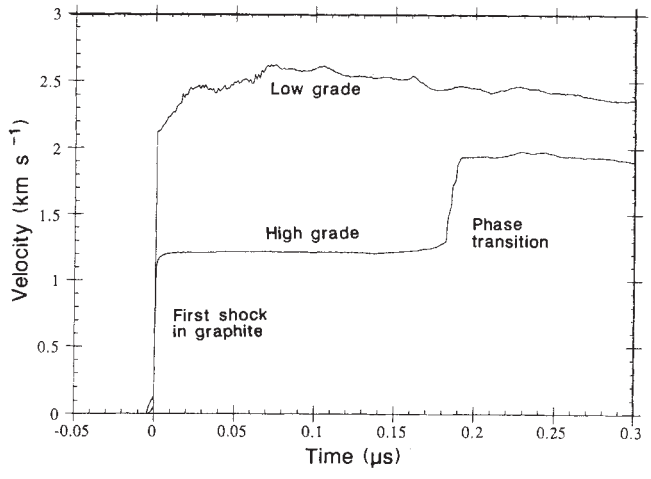

FIG. 1 Velocity profiles of pyrolytic graphite shocked parallel to the c axis of the graphite crystal structure and measured at the graphite–LiF interface for high-grade (shot g2) and low-grade (shot g5) samples. Target g2 was impacted by a 3-mm-thick copper disk at 2.69 km s^{-1}, and target g5 by a 2-mm-thick disk at 3.57 km s^{-1}. The high-grade sample shows a distinct two-wave structure. The first wave indicates the shock compression of graphite to 21 GPa. The second wave indicates a rapid (~10 ns) martensitic transformation to a diamond-like density. The time separation between the two waves is not caused by time latency of the transformation, but by the slower speed of the second wave through the material owing to the increased compressibility at the phase transition. The low-grade sample shows a frustrated transition over several tens of nanoseconds. The final density is significantly less than that of diamond at the same shock pressure, suggesting a complex intermediate state.

Three shots of each grade were fired. Figure 1 shows velocity histories for high- and low-grade samples. The two-wave nature of the high-grade shot is direct evidence for a fast transformation. In the first wave the graphite is shock-compressed to P_{0t}, which is calculated through standard analysis to be 21 GPa (20 and 22 GPa for the other two shots). In the second wave the graphite is compressed in the transformation to a denser phase, calculated to have density $\rho = 3.63$ g cm^{-3}, at a pressure $P = 30$ GPA. Comparison to the density of shocked diamond[21] ($\rho = 3.72$ g cm^{-3} at 30 GPa) suggests that transformation to diamond was nearly complete. The rapid rise (~10 ns) of the second wave in the high-grade sample is evidence for a martensitic transition. The estimated shock temperature of 1,800 K, calculated below, is in the stability field of hexagonal diamond[9].

The wave history of the low-grade sample shows relatively sluggish kinetics, a higher velocity at the onset of the transition, and thus a greater P_{0t} of 42 GPa (31 and 24 GPa for the other shots.) Its second shock state, $\rho = 3.36$ g cm^{-3} at $P = 49$ GPa, is significantly less dense than diamond ($\rho \approx 3.8$ g cm^{-3}) at 49 GPa. The second-shock state is probably a dense, disordered phase. Evidently, the phase-change behaviour of pyrolytic graphite is very sensitive to the degree of orientational order in the specimen.

The temperature of crystal-density graphite shocked to $P_{0t} = 21 \pm 1$ GPa was calculated to be $T \approx 500$–550 K by integrating $dT = (V_0 - V)dP/2C_v + [P/2C_v - T\gamma/V]dV$ along the graphite pressure–volume shock adiabat[14,22]. Here $C_v(T)$, the heat capacity, is taken from ref. 23. The Gruneisen γ was assumed to range between its graphite and diamond values[24], $\gamma = 0.35$ and $\gamma = 1.15$ respectively. The temperature of the second shocked state for the high-grade sample was estimated to be $T \approx 1{,}800$ K via the relation $\Delta T = \Delta P/(\rho\gamma C_v)$, where $\Delta P \approx 13$ GPa is the thermal pressure, the difference between the actual pressure and the diamond cold-compression curve[25] at that density, with $\gamma = 1.15$ and $C_v = 2.0$ J K^{-1} g^{-1} (ref. 26). This calculation assumes 100% conversion to diamond. These temperatures are sufficiently low relative to the melting temperature, and the time duration of the phase transformation sufficiently short (10 ns), that the rapid transition which we observe can be explained only by a martensitic transformation. □

Received 7 August; accepted 6 December 1990.

1. Hanneman, R. E., Strong, H. M. & Bundy, F. P. *Science* **155,** 995–997 (1967).
2. Clarke, R. S., Appleman, D. E. & Ross, D. R. *Nature* **291,** 396–398 (1981).
3. Greiner, N. R., Phillips, D. S., Johnson, J. D. & Volk, F. *Nature* **333,** 440–442 (1988).
4. Lyamkin, A. I. *et al. Sov. Phys. Dokl.* **33,** 705–706 (1988).
5. Decarli, P. S. & Jamieson, J. C. *Science* **133,** 1821–1822 (1961).
6. Cowan, G. R., Dunnington, B. W. & Holtzman, A. H. US Patent No. 3,401,019 (1968).
7. Kurdyumov, A. V., Ostrovskaya, N. F. & Pilyankevich, A. N. *Sov. Powder Metall. Metal Ceram.* **27,** 32–37 (1988).
8. Staver, A. M., Gubareva, N. V., Lyamkin, A. I. & Petrov, E. A. *Sov. Combustion, Explosion and Shock Waves* **20,** 567–570 (1985).
9. Bundy, F. P. & Kasper, J. S. *J. chem. Phys.* **46,** 3437–3446 (1967).
10. Williamson, R. L. *J. appl. Phys.* **68,** 1287–1296 (1990).
11. Coleburn, N. L. *J. chem. Phys.* **40,** 71–77 (1964).
12. Doran, D. G. *J. appl. Phys.* **34,** 844–851 (1964).
13. Pavlovskii, M. N. & Drakin, V. P. *Sov. Phys. JETP Lett.* **4,** 116–118 (1966).
14. McQueen, R. G. & Marsh, S. P. in *Behavior of Dense Media Under High Dynamic Pressures* (Gordon and Breech, New York, 1968).
15. Gust, W. H. *Phys. Rev.* B **22,** 4744–4756 (1980).
16. Pyaternev, S. V., Pershin, S. V. & Dremin, A. N. *Sov. Combustion, Explosion and Shock Waves* **22,** 756–761 (1986).
17. Zeldovich, Ya. B. & Raizer, Yu. P. *Physics of Shock Waves and High-Temperature Hydrodynamic Phenomena,* 750–756 (Academic, New York, 1967).
18. Gogulya, M. F. *Sov. Combustion, Explosion and Shock Waves* **25,** 87–95 (1989).
19. Hemsing, W. F. *Rev. Sci. Instrum.* **50,** 73–78 (1979).
20. Reynolds, W. N. *Physical Properties of Graphite,* 3–5 (Elsevier, Amsterdam, 1968).
21. Pavlovskii, M. N. *Sov. Phys. Solid. St.* **13,** 741–742 (1971).
22. McQueen, R. G., Marsh, S. P. & Fritz, J. N. *J. Geophys. Res.* **72,** 4999–5036 (1967).
23. Morgan, W. C. *Carbon* **10,** 73–79 (1972).
24. van Thiel, M. & Ree, F. H. *Int. J. Thermophysics* **10,** 227–236 (1989).
25. Aleksandrov, I. V., Goncharov, A. F., Zisman, A. N. & Stishov, S. M. *Sov. Phys. JETP* **66,** 384–390 (1987).
26. Touloukian, Y. S. (ed.) *Thermophysical Properties of High Temperature Solid Materials* Vol. 1, 394 (Macmillan, New York, 1967).

ACKNOWLEDGEMENTS. We thank F. P. Bundy, A. N. Dremin and M. F. Gogulya for helpful discussions. This work was performed under the auspices of the US Department of Energy by the Lawrence Livermore National Laboratory.

Direct measurement of nitrogen gas fluxes from continental shelf sediments

Allan H. Devol

School of Oceanography, WB-10, University of Washington, Seattle, Washington 98195, USA

IT has been suggested that denitrification in continental shelf and slope sediments is the most important sink in the marine nitrogen cycle[1–4]. This conclusion has been reached, not from direct measurements of denitrification in these areas, but rather from indirect estimates derived from pore-water models of diagenetic processes. In highly bioturbated continental shelf and slope sediments with steep pore-water gradients, such indirect estimates may not be applicable[5,6]. I have now made direct, *in situ* measurements of denitrification in sediments of the eastern North Pacific continental margin by determining the flux of molecular nitrogen out of the sediments into the overlying water. Denitrification rates in continental shelf sediments measured in this fashion averaged 3.7 pmol N cm^{-2} s^{-1}. The flux of nitrate from the overlying water into the sediments was only 1.5 pmol N cm^{-2} s^{-1}, showing that most of the nitrogen gas production is coupled to nitrification within the sediments. The denitrification rates observed here are four to five times those estimated previously by indirect methods for these same sediments, and indicate the limitations of such indirect estimates. My results suggest that the global denitrification rate in shelf and slope sediments may be greater than previously thought, and confirm the importance of sedimentary denitrification in the marine nitrogen budget.

Denitrification is the process whereby combined nitrogen, principally NO_3^-, is used as the oxidant for organic matter and the nitrogen is reduced to N_2 (ref. 7). Denitrification takes place in the absence, or near absence of dissolved oxygen[8] and is the major sink term in the marine budget of combined nitrogen. Inputs to the budget include atmospheric precipitation (40 Tg yr^{-1}), riverine input (25 Tg yr^{-1}) and *in situ* nitrogen fixation (25 Tg yr^{-1}). These inputs are balanced by losses due to permanent burial in marine sediments (20 Tg yr^{-1}), denitrification (70–145 Tg yr^{-1}) and miscellaneous other processes (15 Tg yr^{-1})[1,2]. Thus, depending on the true value of the

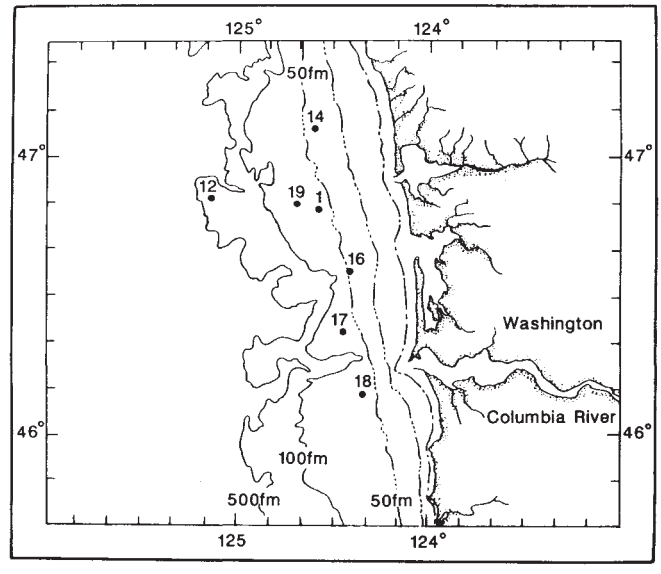

FIG. 1 Location of stations at which fluxes of N_2 and NO_3^- were measured.